Influences of Material Degradation Due to Laser Cutting on the Operating Behavior of PMSM Using a Continuous Local Material Model

Silas Elfgen, Simon Steentjes, Stefan Böhmer, David Franck, and Kay Hameyer, *Senior Member, IEEE*

***Abstract*—During manufacturing of electrical machines, shape giving production steps such as punching and cutting introduce plastic deformations and residual stress to the soft magnetic material. As a result, the magnetic properties of the material decrease and locally both static and dynamic hysteresis losses increase in the vicinity of the cut surfaces. For consideration of local permeability deteriorations, different models have been published. These are capable of describing the changing local magnetization and loss behavior. Current approaches subdivide the magnetic core into slices of different magnetic properties, thereby discretizing the continuous deterioration. This paper analyzes the effects of material degradation due to cutting on the performance and machine parameters of a permanent magnet synchronous machine using a continuous material model for efficient numerical modeling of the local magnetization behavior. By replacing inefficient sliced models, the continuous model is independent of the discretization and converges in case of coarse meshes to the sliced model. Influences on the machine behavior are studied in terms of local flux density distributions, iron losses, efficiency, torque, and inductances on the operating map and an exemplary working point.**

***Index Terms*—Continuous material model, cut edge (CE), cutting, iron losses, permanent magnet synchronous machine (PMSM), soft magnetic material.**

I. Introduction

NONGRAIN oriented soft magnetic material is one of the key components considering the energy conversion in rotating electrical machines. Laminations of nonoriented steels are used both in stator and rotor. In order to gain high power density current permanent magnet synchronous machines (PMSM) work with a high flux in the air gap and, therefore, high flux densities in stator and rotor parts. Additionally, nonoriented steels with low iron losses are used to increase efficiency. During manufacturing the laminations are punched out of the coil to the desired shape. Attention has to be paid not only to the design but also on the cutting technique itself [1], [2]. Studies on different manufacturing techniques such as laser cutting for prototyping or stamping during production demonstrate the negative influence on the local magnetic characteristics.

The effects of manufacturing processes on the local resulting iron losses differ depending on their parameters. These are in case of stamping, e. g., clearance, cutting speed, or the condition of the blade. In case of laser cutting parameters such as laser type, focus width, energy, and cutting speed are important. A considerable difference is found in view of resulting iron losses comparing uncut and cut material [3]–[5]. Depending on geometrical, material, and processing parameters along with the magnetic field strength, the iron losses resulting from different cutting techniques can differ by a factor of two or higher, due to increasing static and dynamic losses [2], [3], [5], [6].

On that account, determining the local magnetic properties of soft magnetic materials used in electrical machines is critical to an improved design process using finite element (FE) simulations. The different cutting techniques introduce mechanical stress into the material, resulting in a locally decreasing magnetic permeability [7]–[10].

In order to cope with continuous, locally changing material properties different models have been published describing local permeability distributions [11]–[13] or aiming at the resulting iron losses [14]. Current attempts discretize coarsely the continuous local material properties by subdividing the iron core of a model into slices [12], [13], [15]. The different material properties are homogeneous across the corresponding slices. Therefore, the sliced approach lacks due to the constant material properties inside the subdivision in accuracy and converges with a sufficient amount of layers to the continuous model [16]. Moreover, a complicated modeling of slices arises during preprocessing. In light of these drawbacks, this paper uses a continuous material model published in [17] to investigate the influences of cut edge (CE) effects on the machine parameters and performance using PMSM. The CE model is established in the numerical FE simulation to describe locally distributed magnetic material properties.

The paper is structured as follows. Section II contains a brief explanation of the metrological characterization performed to identify model and loss parameters, followed by an overview on the nominal machine parameters and geometrical data. Subsequently, the continuous material model is explained briefly and model parameters are identified. Section III concerns the

Manuscript received September 16, 2016; revised December 8, 2016; accepted January 27, 2017. Date of publication February 7, 2017; date of current version May 18, 2017. Paper 2016-EMC-0981.R1, presented at the 2016 22nd International Conference on Electrical Machines, Ecublens, Switzerland, Sep. 4–7, and approved for publication in the IEEE TRANSACTIONS ON INDUSTRY APPLICATIONS by the Electric Machines Committee of the IEEE Industry Applications Society.

The authors are with the Institute of Electrical Machines, RWTH Aachen University, Aachen 52062, Germany (e-mail: silas.elfgen@iem.rwth-aachen.de; simon.steentjes@iem.rwth-aachen.de; stefan.boehmer@iem.rwth-aachen.de; david.Franck@iem.rwth-aachen.de; k.h@iem.rwth-aachen.de).

Color versions of one or more of the figures in this paper are available online at http://ieeexplore.ieee.org.

Digital Object Identifier 10.1109/TIA.2017.2665338

continuous material model used in FE simulations and a comparison of the resulting local flux density distribution in an CE affected and unaffected case. Iron loss parameters are identified according to different specimen widths and frequencies and loss calculations are carried out on the operating map. In Section IV, machine parameters are investigated in terms of iron losses, efficiency, torque and inductances. A discussion on the results is given in Section V.

II. Continuous Modeling of CE Effects in a Rotating Machine

A. Material Sample Preparation

With the aim to model local magnetization behavior in FE simulations for a rotating machine continuously, it is necessary to characterize different material samples for model parameter identification. The material used here is a nonoriented M330-35 A, with Si 2.9%, Al 0,4%, P 10_{ppm}, Mn 0,13%, C 29 ppm, S 39 ppm, and an average grain size of 80 μm. It is cut by a CO_2-Laser with a gas pressure of 10 bar, using a speed of $8\frac{\mathrm{m}}{\mathrm{min}}$, a power of 1700 W and a focus of a 5 in lens.

Single sheet laminations with different amount of cuts are characterized as demonstrated in [17] to measure magnetic properties according to the material width of the machine design. The width of each specimen set, is equaling 120 mm in total. Starting with a basic sheet of 120 mm $\times$ 120 mm samples with smaller width are consecutively cut out of the basic square. Thereby, single samples equaling a width b of 120, 60, 30, 15, 10, 5 and 4 mm are produced.

The material samples are magnetically characterized according to the IEC standard 60404 using a single sheet tester (SST) with a specimen size of 120 $\times$ 120 mm, 50 windings and the control unit MPG200 both by Brockhaus. While performing the measurements, the secondary voltage is controlled by an analogous system to be sinusoidal, as well as the maximum magnetic Polarization $\hat{J}$. Frequencies are measured for dc, 50, 100, 200, 400, 500, 700 Hz and 1 kHz and flux densities up to 1,6T. The form factor FF rises with decreasing specimen width and increasing frequency and polarization. It lies in the norm defined range at least for frequencies and polarizations below 400 Hz and 1.5 T, respectively.

Loss parameter and model parameter identification are both carried out on the single sheet specimens at the different frequencies. A comparison of measured and calculated losses of FE simulations using toroidal cores is drawn in [17].

B. Machine Data

It is well known that CE effects get more pronounced with smaller geometrical sizes [18]. Therefore a small PMSM with stator outer diameter $D_{S,o}$ of 90 mm is used for analyzing the effect of local material degradation on the machine performance. As mentioned, current PMSMs already work at high flux densities in a no-load case. Although CE effect on the magnetization behavior decrease with rising field strength, still a changed local flux density distribution and a considerable increase in iron losses is expected due to the small geometrical sizes of, e.g., stator teeth $w_{S,t}$ and yoke $w_{S,y}$ [5]. A cross section of the studied machine geometry is depicted in Fig. 1 and the corresponding geometrical sizes are given in Table I. The machine has a nominal power P_n of 180 W, an efficiency η_n of 82.5% and is constructed with distributed windings. The rotor is shaped in a sinusoidal way with buried permanent magnets. Corresponding machine characteristics at the nominal working point are given in Table II provided by the manufacturer.

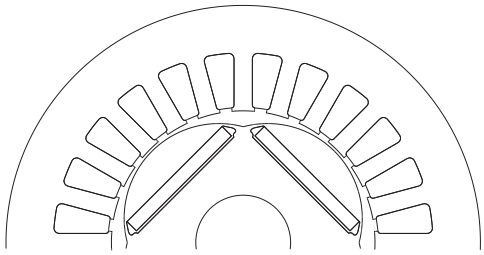

Fig. 1. Cross section of the machine geometry.

TABLE I
Geometrical Data

Parameter	Symbol	Value
Stator outer diameter	$D_{S,o}$	90×10^{-3} m
Rotor outer diameter	$D_{R,o}$	49×10^{-3} m
Stator tooth width	$w_{S,t}$	4.2×10^{-3} m
Yoke width	$w_{S,y}$	9×10^{-3} m
Slots	N	24
Pole pairs	p	2

TABLE II
Machine Characteristics of Nominal Working Point

Parameter	Symbol	Value
Speed	n_n	1500 min^{-1}
Power	P_n	219 W
Torque	M_n	1,44 N·m
Efficiency	η_n	82.50%
Iron losses	$P_{\mathrm{fe},n}$	5 W
Copper losses	$P_{\mathrm{cu},n}$	40 W

C. Material Model

The CE model published in [16] and [19] describes the local permeability $\mu_r(H,x)$ as function of the magnetic field strength H, the unaffected relative magnetic permeability μ_r and the distance to the cut edge x.

$$\mu_r(H,x) = \mu_r(H) - \Delta\mu_{\mathrm{cut}}(H) \cdot \eta(x,\delta,a). \tag{1}$$

The continuous model is defined by three model parameters, whereof $\Delta\mu_{\mathrm{cut}}$ describes the maximum permeability drop at the CE ($x = 0$), δ the depth of the CE affected material and a the inclination of the local permeability profile $\eta(x)$. Both parameters a and δ are contained in local permeability profile. For distances of $x > \delta$ the material is considered to be unaffected. An unaffected material property is described by the

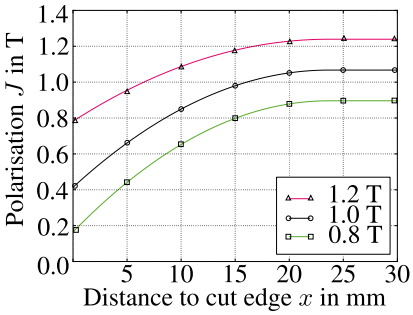

Fig. 2. Local magnetic polarization J at different mean flux densities.

relative permeability μ_r. Model parameters are identified from single sheet measurements of different strip width mentioned in Section II-A. For parameter identification a specimen strip width of 120 mm is considered to be unaffected by the CEs.

With a locally depending permeability description in (1) it is possible to assign a local magnetization behavior $\mu(H, x)$ to each element of the FE mesh according to its distance to the CE x. For simulation the reluctivity $\nu(B^2, x)$ corresponding to distances x from the CE is stored in matrix form as shown in (2). The results of the of iron losses are consistently influenced by the results of the local permeability model, but iron loss calculation are independent of the local material model and, therefore, described in Section III-B.

$$\begin{pmatrix} \nu(B_1^2, x_1) & \cdots & \nu(B_1^2, x_n) \\ \vdots & \ddots & \\ \nu(B_n^2, x_1) & & \nu(B_n^2, x_n) \end{pmatrix}. \tag{2}$$

By taking an exemplary strip width, Fig. 2 demonstrates the local polarization $J(H, x)$ at different levels of mean polarization. The mean values of the local polarization correspond with measured values of a single sheet measurement.

III. Simulation

The simulation of the PMSM operating map is performed using a current density matrix of 13×13 values. The sampling points of direct and quadrature current are $I_d = -6, 0{\cdot}10^6 \frac{\mathrm{A}}{\mathrm{m}^2}$ to 0.0 $\frac{\mathrm{A}}{\mathrm{m}^2}$ and $I_q = 0.0 \frac{\mathrm{A}}{\mathrm{m}^2}$ to $6.0{\cdot}10^6 \frac{\mathrm{A}}{\mathrm{m}^2}$ in steps of $0.5{\cdot}10^6 \frac{\mathrm{A}}{\mathrm{m}^2}$. Every operating point is calculated with a resolution of 90 steps per electrical period. The distance to CE of every FE element is stored as additional information on the mesh. During processing the corresponding reluctivity values of the current FE element is extracted from the material matrix shown in (2) by interpolating between the reference points of the matrix entries. Calculations are done for both an unaffected and a CE affected magnetization behavior. Results of both types are discussed in the following, starting with the local flux density and the resulting iron losses.

A. Local Flux Density Distribution

An exemplary working point is selected from the operating area to demonstrate the effect of material degradations due to CEs on the local flux density distribution and related local and total iron losses. The selected operating point is within the area of field weakening. Therefore lower flux density's are inside the stator tooth.

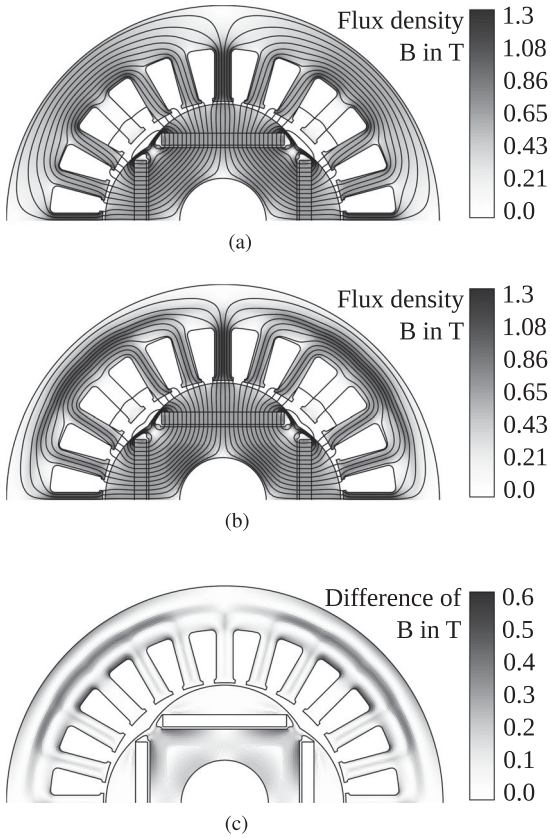

Fig. 3. Local flux density distribution and vector potential considering (a) an unaffected, (b) a CE affected magnetization characteristic, and (c) the absolute difference of the local flux density solutions in an exemplary working point. (a) Unaffected flux density solution. (b) CE affected solution considering the continuous material model. (c) Absolute difference between unaffected and CE affected solution $B_{\mathrm{unaffected}}(x) - B_{\mathrm{CE}}(x)$.

In Fig. 3 the local flux density distribution along with the flux lines are shown for an unaffected and a CE affected solution. The solution with an unaffected magnetization behavior in Fig. 3(a) shows that maximum local flux density in stator tooth and yoke are both low, reaching 1.1 T and 0.65 T, respectively. The flux density is distributed almost equally across the yoke and tooth diameter. In case of the CE affected magnetization behavior in Fig. 3(b), maximum local flux density in stator tooth and yoke reach 1.3 T and 1.0 T, respectively. Due to the locally damaged material at the edges and consequently decreased magnetic permeability, a concentration of the flux into the center of the tooth and yoke can be observed. To illustrate the effect Fig. 3(c) depicts the absolute difference of the local flux density solutions $B_{\mathrm{unaffected}}(x) - B_{\mathrm{CE}}(x)$. Along with that a slightly lower amount of rotor stray flux in the magnetic q-axis between the pockets of the permanent magnets is observed. On the other hand, the flux concentration inside yoke and tooth results into a higher flux density at the back of the stator tooths. During operation the flux maximum follows an elliptic shape [20]. An increasing flux density at the tooth back will lead to higher eddy-current and excess losses in this area. Consequently, the change of local losses distribution will be discussed in the following.

B. Iron Loss Calculation

Iron loss calculations are performed according to [21] using (3). Loss separation is done in terms of hysteresis losses using parameter a_1 and α, classic eddy-current losses a_2, and additional losses a_5. In order to cope with rising losses at high frequencies and high flux densities, the phenomenological contribution of the nonlinear material behavior is added using loss parameter a_3 and a_4.

With decreasing material width a considerable increase in measured static hysteresis losses can be noticed which is in accordance with [5] and [9]. It is assumed that static hysteresis losses are most affected by cutting [5], [19]. Loss parameters are identified according to the different SST specimens listed in Section II-A, respectively. Aside from hysteresis loss parameters a_1 and α no analytical consistent description between strip width b and the loss parameters is found. In [17], the applicability of the strip width depended loss parameter is demonstrated using ring core specimens. This approach is transferred to the current machine design, with static hysteresis losses in (3), calculated dependent on the strip width $a_1(b)$ and $\alpha(b)$.

$$P_{\mathrm{IEM},5} = P_{\mathrm{hyst}} + P_{\mathrm{classical}} + P_{\mathrm{excess}} + P_{\mathrm{sat}}. \tag{3}$$

The loss contributions are calculated as described in (4)–(7). The flux density B_n is the amplitude of the nth harmonic component of the magnetic flux density, n the order of harmonic, f the fundamental frequency, and r_{hyst}, r_{excess} the rotational loss factors explained in [20]

$$P_{\mathrm{hyst}} = a_1(b)\left[1 + \frac{B_{\min}}{B_{\max}}(r_{\mathrm{hyst}})\right] B_{\max}^{\alpha(b)} f \tag{4}$$

$$P_{\mathrm{classical}} = a_2 \sum_{n=0}^{\infty} (B_n^2 (nf)^2) \tag{5}$$

$$P_{\mathrm{excess}} = a_5\left[1 + \frac{B_{\min}}{B_{\max}}(r_{\mathrm{excess}} - 1)\right] \sum_{n=1}^{\infty} (B_n^{1.5} (nf)^{1.5}) \tag{6}$$

$$P_{\mathrm{sat}} = a_2 a_3 B_{\max}^{a_4+2} f^2. \tag{7}$$

Fig. 4 depicts the identification of $a_1(b)$ and $\alpha(b)$ in dependency on the strip width and the cutting direction relative to the rolling direction. In order to quantify hysteresis loss parameters according to the geometrical dimensions of stator yoke $w_{S,y}$ and tooth $w_{S,t}$ given in Table I, a linear approximation is assumed. Thereby, an equivalent strip width is assigned to the stator and the corresponding loss parameters are determined.

The remaining loss parameters for iron loss calculations are identified considering all specimen widths from Section II-A, at different frequencies. Hysteresis and excess loss calculations on the local flux density solutions are performed considering the ratio between minimal and maximal local flux density $B_{\min}$, $B_{\max}$. Furthermore, higher harmonics of the flux density are taken into account for classic and excess losses by Fourier analysis [20]. As pointed out in Section III-A, a changing local magnetization behavior leads to a changing local loss distribution. The influence in terms of local hysteresis losses are demonstrated in Fig. 5 on the stator geometry. A significant increase in

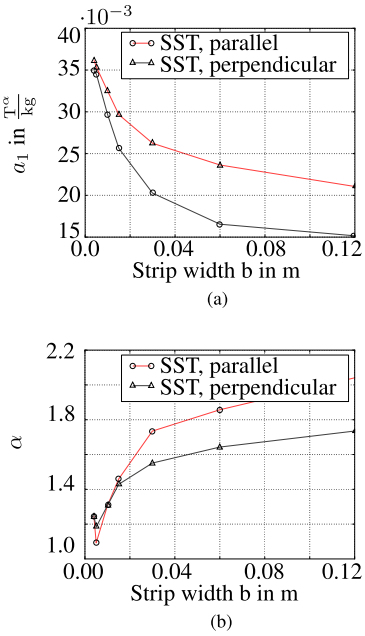

Fig. 4. Identification of (a) $a_1(b)$ and (b) $\alpha(b)$ the hysteresis loss parameter dependent on the strip width.

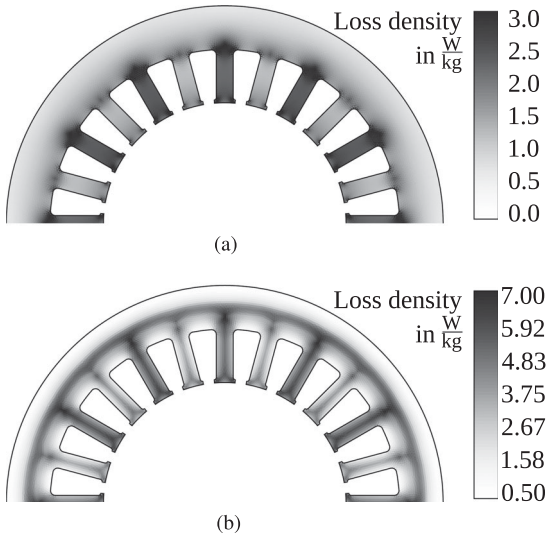

Fig. 5. Local hysteresis loss density distribution in an exemplary working point considering (a) an unaffected and (b) a CE affected material behavior on the stator geometry.

local hysteresis loss density can be observed at the stator tooth back. The increase of losses at the stator tooth back also applies for local classic and excess losses. As a consequence of the flux concentration in stator tooth and yoke, reduced local losses at the edges especially on the yoke outer edge occur. On the contrary, flux concentration to the center of the geometry increases the local hysteresis losses significantly.

IV. Influences on the Operational Behavior

In order to evaluate the effects of CEs on the operational behavior, the PMSM operating map is discussed further. Fig. 6(a) depicts the undamaged efficiency map as presented in [22]. The

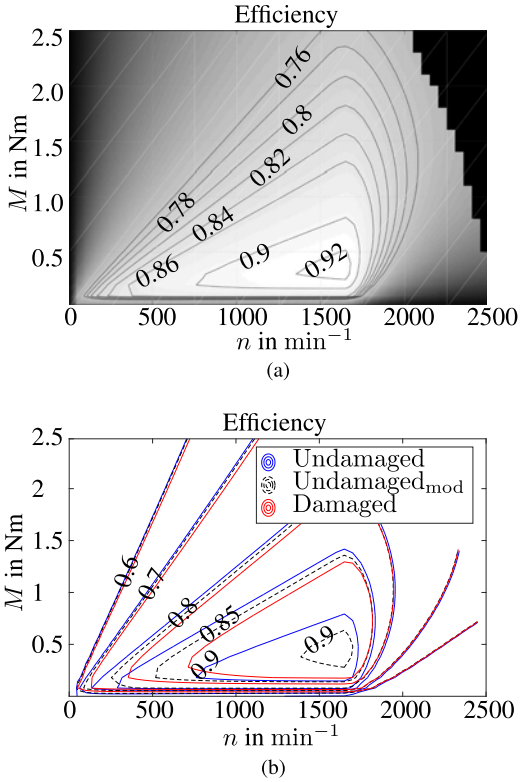

Fig. 6. Efficiency map of (a) the unaffected machine design and (b) of the CE affected machine design along with the efficiency calculated with an undamaged flux density solution and CE effected loss parameters.

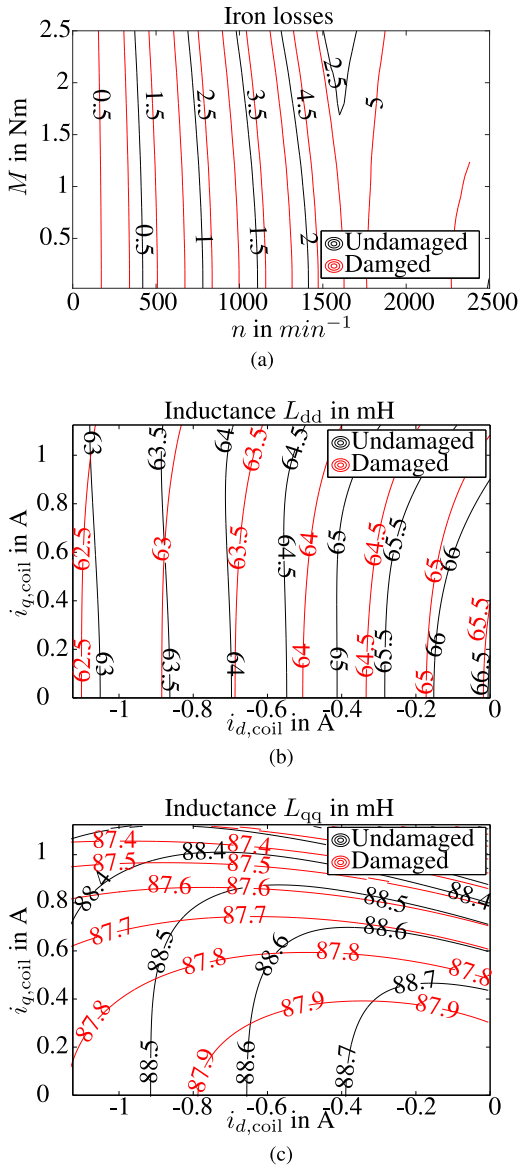

Fig. 7. Contour maps of (a) resulting iron losses, and (b) and (c) the resulting main inductance in magnetic d- and q-axis of the unaffected and CE affected machine design.

Calculations include copper, iron, and friction losses. In addition, Fig. 6(b) demonstrates the difference in efficiency between an unaffected and a CE affected design. The dashed contour plotted in Fig. 6(b) depicts the influence of the local flux density solution on the calculated efficiency. This modified undamaged solution uses the local flux density of tthe undamaged case along with the damaged loss parameters. In comparison it can be seen that the area of maximum efficiency is shrinking toward higher speed and does not reach the maximum efficiency of the unaffected design. Further, the overall efficiency is decreased mainly because of higher iron losses and a rising sensitivity of the efficiency to the local flux density distribution can be seen in the area of higher efficiency.

The influence on the calculated iron losses in the operating map is shown in Fig. 7(a) as a contour plot of both variants. Total iron losses increase significantly depending on the operating point. The CE effect is more pronounced at lower field strength and decreases toward saturation polarization. In particular, in the field weakening range with lower flux densities, higher iron losses due to eddy currents can be observed. Studying the different loss contributions the strongest effect is viewed in terms of hysteresis losses. Nevertheless the other loss contributions are found to increase as well. The influence of the changing flux density solution on the iron losses was also investigated by using the same loss parameters on the unaffected and CE affected solution. Increasing iron losses due to a changed local flux distribution was found to be in the range of 10%. The total calculated torque of a CE affected machine design is slightly reduced. Moreover slightly higher copper losses arise mainly in the base speed range, but the influences on torque and copper losses is below 1%.

The changing magnetization behavior can also be seen in the characteristic of the main inductances in q-axis L_{qq} and d-axis L_{dd}. Fig. 7 shows the influence on the main inductances depending on the current in both cases as a contour plot. Considering L_{dd} at a constant current combination of i_q and i_d, a reduced inductance value is observed across the current map. In case of higher values of i_d, the dependency of the inductance from i_q rises in the case of the CE affected material whereas the dependency on i_d for varying values of i_q stays constant. Considering L_{qq} at a constant current combination of i_q and i_d, a reduced inductance value is observed also across the current map. In case of constant i_q values, a reduced dependency of the inductance from i_d can be observed considering CE affected

TABLE III
COMPARISON OF RESULTING MACHINE PARAMETERS AT NOMINAL WORKING POINT

	Undamaged	Undamage with-CE-effected losses	Damaged	Nominal
P_{Fe}	2.26 W	3.72 W	4.77 W	5 W
P_{Cu}	38.81 W	38.81 W	39.45 W	40.33 W
η	0.842	0.837	0.832	82.5

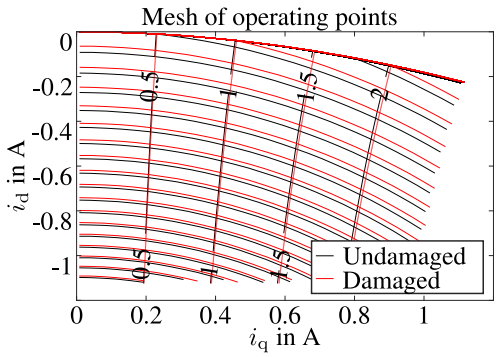

Fig. 8. Contour map of resulting operating points of the unaffected and CE affected machine design with including torque isolines.

material. The smaller inductances are the result of an increasing magnetic resistance of the soft magnetic parts through CEs.

In order to exemplary compare the influence of the changed local flux distribution on the losses and magnetization current, the resulting values of the nominal working point are listed in Table III. The table presents the results of the undamaged solution, damaged solution and nominal values as listed in Table II. Further the combination of the undamaged flux density solution with damaged loss parameters, as presented in Fig. 6(b), is listed to demonstrate the impact of the local flux density model. The increase in iron and copper losses are partly due to the changed local flux density and the adapted loss parameters.

Using a Maximum torque per ampere control strategy the resulting mesh of operating points can be calculated. Fig. 8 depicts the effect of laser cutting on the magnetization current density in both direct and quadrature axis along with isolines of constant torque. As a consequence of the local material degradation, a rising need of the direct current i_{d} can be seen for a constant operating point. The influence is more pronounced for low direct currents and nearly constant for rising torque values. Consistently, slightly higher iron losses result as listed in Table III.

V. CONCLUSION

The influences of CEs due to laser cut on the operating behavior of an exemplary PMSM machine design were studied. The CE effect is described by a continuous model to consider local magnetic material degradation. Model parameters are identified by single sheet measurements using specimens of different strip width. The resulting iron loss parameters are identified on single sheet specimens of different strip width and different frequencies according to the operating range of the machine. A coherent dependency of the different loss parameters on the strip width is found only in case of the hysteresis parameter. With respect to the geometrical dimensions of the machine design loss parameters are determined.

Further, the influences on the machine are studied on the operating map and in an exemplary working point. Due to the locally damaged material at the CEs, a considerable flux concentration to the center of the soft magnetic material can be observed. As a consequence of the changing local flux density distributions and increasing hysteresis loss parameters due to smaller material widths, a changing local loss distributions inside the machine can be observed. Iron losses rise significantly across the operating map lowering the overall machine efficiency and the maximum efficiency of the unaffected machine can not be reached.

Influences of CEs on the torque are found to be low. The main inductances are lowered by an increased magnetic resistance of the soft magnetic parts. Depending on the degree of magnetic deterioration CEs considerably affect machine behavior. In particular, in the case of geometrically smaller machine designs the importance of considering local magnetization behavior is demonstrated.

REFERENCES

[1] A. Moses, N. Derebasi, G. Loisos, and A. Schoppa, "Aspects of the cut-edge effect stress on the power loss and flux density distribution in electrical steel sheets," *J. Magn. Magn. Mater.*, vol. 215–216, pp. 690–692, 2000.

[2] P. Baudouin, M. D. Wulf, L. Kestens, and Y. Houbaert, "The effect of the guillotine clearance on the magnetic properties of electrical steels," *J. Magn. Magn. Mater.*, vol. 256, no. 1–3, pp. 32–40, Jan. 2003.

[3] M. Hofmann, H. Naumoski, U. Herr, and H. Herzog, "Magnetic properties of electrical steel sheets in respect of cutting: Micromagnetic analysis and macromagnetic modeling," *IEEE Trans. Magn.*, vol. 52, no. 2, pp. 1–14, Feb. 2016.

[4] G. Crevecoeur, P. Sergeant, L. Dupre, L. Vandenbossche, and R. van de Walle, "Analysis of the local material degradation near cutting edges of electrical steel sheets," *IEEE Trans. Magn.*, vol. 44, no. 11, pp. 3173–3176, Nov. 2008.

[5] S. Steentjes, G. von Pfingsten, and K. Hameyer, "An application-oriented approach for consideration of material degradation effects due to cutting on iron losses and magnetizability," *IEEE Trans. Magn.*, vol. 50, no. 11, pp. 416–417, Nov. 2014.

[6] A. Schoppa, J. Schneider, and C.-D. Wuppermann, "Influence of the manufacturing process on the magnetic properties of non-oriented electrical steels," *J. Magn. Magn. Mater.*, vol. 215/216, no. 0, pp. 74–78, 2000.

[7] F. Ossart, E. Hug, O. Hubert, C. Buvat, and R. Billardon, "Effect of punching on electrical steels: Experimental and numerical coupled analysis," *IEEE Trans. Magn.*, vol. 36, no. 5, pp. 3137–3140, Sep. 2000.

[8] G. Loisos and A. J. Moses, "Effect of mechanical and Nd:YAG laser cutting on magnetic flux distribution near the cut edge of non-oriented steels," *J. Mater. Process. Technol.*, vol. 161, no. 1/2, pp. 151–155, 2005, 3rd Japenese-Mediterranean Workshop on Applied Electromagnetic Engineering for Magnetic and Superconducting Materials and 3rd Workshop on Superconducting Flywheels.

[9] H. Naumoski, A. Maucher, L. Vandenbossche, S. Jacobs, U. Herr, and X. Chassang, "Magneto-optical and field-metric evaluation of the punching effect on magnetic properties of electrical steels with varying alloying content and grain size," in *Proc. 4th Int. Elect. Drives Prod. Conf.*, Sep. 2014, pp. 1–9.

[10] R. Siebert, A. Wetzig, E. Beyer, B. Betz, C. Grunzweig, and E. Lehmann, "Localized investigation of magnetic bulk property deterioration of electrical steel: Analysing magnetic property drop thorough mechanical and laser cutting of electrical steel laminations using neutron grating interferometry," in *Proc. 3rd Inter. Elect. Drives Prod. Conf.*, Oct. 2013, pp. 1–5.

[11] K. Fujisaki *et al.*, "Motor core iron loss analysis evaluating shrink fitting and stamping by finite-element method," *IEEE Trans. Magn.*, vol. 43, no. 5, pp. 1950–1954, May 2007.
[12] M. Bali, H. De Gersem, and A. Muetze, "Finite-element modeling of magnetic material degradation due to punching," *IEEE Trans. Magn.*, vol. 50, no. 2, pp. 745–748, Feb. 2014.
[13] L. Vandenbossche, S. Jacobs, X. Jannot, M. McClelland, J. Saint-Michel, and E. Attrazic, "Iron loss modelling which includes the impact of punching, applied to high-efficiency induction machines," in *Proc. 3rd Int. Elect. Drives Prod. Conf.*, Oct. 2013, pp. 1–10.
[14] B. Hribernik, "Influence of cutting strains on the magnetic anisotropy of fully processed silicon steel," *J. Magn. Magn. Mater.*, vol. 26, no. 1–3, pp. 72–74, 1982.
[15] Z. Gmyrek and A. Cavagnino, "Analytical method for determining the damaged area width in magnetic materials due to punching process," in *Proc. 37th Annu. Conf. IEEE Ind. Electron. Soc.*, Nov. 2011, pp. 1764–1769.
[16] S. Elfgen, S. Böhmer, S. Steentjes, D. Franck, and K. Hameyer, "Continuous model of magnetic material degradation due to cutting effects in the numerical simulation of electro laminations," in *Proc. 10th ETG/GMM-Symp. Innov. Small Drives Micro-Motor Syst.*, Sep. 2015, pp. 1–6.
[17] S. Elfgen, S. Steentjes, S. Bhmer, D. Franck, and K. Hameyer, "Continuous local material model for cut edge effects in soft magnetic materials," *IEEE Trans. Magn.*, vol. 52, no. 5, pp. 1–4, May 2016.
[18] A. Schoppa, J. Schneider, and C.-D. Wuppermann, "Influence of the cutting process on the magnetic properties of non-oriented electrical steels," *J. Magn. Magn. Mater.*, vol. 215/216, pp. 100–102, 2000.
[19] L. Vandenbossche, S. Jacobs, F. Henrotte, and K. Hameyer, "Impact of cut edges in magnetization curves and iron losses in e-machines for automotive traction," in *Proc. 25th World Battery, Hybrid Fuel Cell Elect. Veh. Symp. Exhibit.*, Schenzhen, China, Nov. 2010, pp. 587–596.
[20] S. Steentjes, D. Eggers, M. Leßmann, and K. Hameyer, "Iron-loss model for the FE-simulation of electrical machines," in *Proc. Inductica Tech. Conf.*, Berlin, Germany, Jun. 2012, pp. 239–246.
[21] D. Eggers, S. Steentjes, and K. Hameyer, "Frequency dependency of nonlinear loss parameter for an improved iron loss prediction," in *Proc. 21st Int. Conf. Soft Magn. Mater*, Budapest, Hungary, Sep. 2013, Paper. 254.
[22] S. Elfgen, S. Steentjes, S. Böhmer, D. Franck, and K. Hameyer, "Influences of material degradation due to laser cutting on the operating behaviour of PMSM using a continuous local material model," in *Proc. 2016 22nd Int. Conf. Elect. Mach.*, Sep. 2016, pp. 1835–1840.

Silas Elfgen received the M.Sc. degree in electrical engineering from RWTH Aachen University, Aachen, Germany, in 2013.

He has been working as a Research Associate with the Institute of Electrical Machines, RWTH Aachen University. His research interests include soft magnetic material, simulation, and performance improvement of the electrical machines.

Simon Steentjes received the diploma degree in electrical engineering from RWTH Aachen University, Aachen, Germany, in 2011.

Since December 2011, he has been working as a Research Associate with the Institute of Electrical Machines, RWTH Aachen University. His research interests include hard- and soft magnetic material modeling on the micro- and macroscopic scale, iron loss calculation, effects of material processing, magnetic forces, and mathematical methods.

Stefan Böhmer received the diploma degree in computer science from RWTH Aachen University, Aachen, Germany, in November 2010.

He has been working as a Research Associate with the Institute for Electrical Machines, RWTH Aachen University. His research interests include numerical field computation and simulations of electrical machines and power converters.

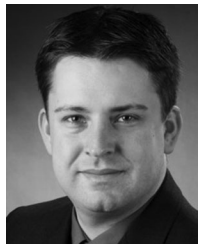

David Franck received the Dipl.-Ing. degree in electrical engineering from RWTH Aachen University, Aachen, Germany, in 2008.

He was a Research Associate at the Institute of Electrical Machines, RWTH Aachen University, where since 2011, he has been working as a Chief Engineer. His main field of research is acoustic of the electrical machines.

Kay Hameyer (M'96–SM'99) received the M.Sc. degree in electrical engineering from the University of Hannover, Hannover, Germany, in 1986 and the Ph.D. degree in design of electrical machines from the University of Technology Berlin, Berlin, Germany, in July 1992.

After his university studies, he was at Robert Bosch GmbH, Stuttgart, Germany, as a Design Engineer for permanent-magnet servo motors and electrical board net components for vehicles. Until February 2004, he was a Full Professor of numerical field computations and electrical machines at Katholieke Universiteit Leuven, Leuven, Belgium. Since 2004, he has been a Full Professor, the Director of the Institute of Electrical Machines, and the holder of the Chair of Electromagnetic Energy Conversion with RWTH Aachen University, Aachen, Germany, where he was the Dean of the Faculty of Electrical Engineering and Information Technology from 2007 to 2009. His research interests include numerical field computation and simulation; design of electrical machines, particularly permanent-magnet excited machines and induction machines; and numerical optimization strategies.